The topological significance of saddle point van Hove singularities: a comparison of orbital switching and magnetic breakdown

1994 J. Phys.: Condens. Matter 6 3059

(http://iopscience.iop.org/0953-8984/6/16/011)

J. Phys.: Condens. Matter 6 (1994) 3059–3072. Printed in the UK

The topological significance of saddle point van Hove singularities: a comparison of orbital switching and magnetic breakdown

R S Markiewicz

Physics Department and Barnett Institute, Northeastern University, Boston, MA 02115, USA

Received 5 May 1993, in final form 5 January 1994

Abstract. The saddle point van Hove singularity has a topological interpretation in terms of a switching of electron orbits from electron like to hole like. This orbital switching bears some resemblance to magnetic breakdown, but is clearly a distinct phenomenon. The tunnelling probability for orbital switching is calculated, and the results compared to magnetic breakdown. Just as in magnetic breakdown, the electronic orbits can form a *quantum coherent network* in the presence of finite orbit switching.

1. Introduction

The saddle point van Hove singularity (vHs) of a two-dimensional electronic band has been implicated as a possible cause for high-temperature superconductivity [1–6]. Here, I discuss a novel topological characteristic of the vHs, which can have an important effect on many of its physical properties. The vHs acts as an *orbital switch*, causing electrons to switch over from one orbit to a distinct one. Precisely at the vHs, the probability of remaining on the same orbit and the probability of switching orbits are both equal to one half.

In the semiclassical picture, the switching probability jumps discontinuously from zero to one as the Fermi level passes the switching orbit. This picture must be corrected by the inclusion of tunnelling processes, which can couple the orbits even when the Fermi level is not precisely at the switching point. Such tunnelling will be present in zero magnetic field, assisted by phonons. However, the resulting strong electron–phonon coupling makes the tunnelling process difficult to analyse. In this paper, I will study the simpler process of magnetic-field-enhanced tunnelling, and only in the final section make some remarks on phonon-enhanced tunnelling.

Field-enhanced orbital switching bears a certain resemblance to conventional magnetic breakdown [7–9], a resemblance which can be utilized to simplify many of the calculations. However, there is a distinction between orbital switching and magnetic breakdown, which can be best understood by analysing a quasi-one-dimensional (quasi-1D) example. Figure 1 illustrates a series of Fermi surfaces, at increasing values of energy, for a nearly free electron model of a material with a rectangular unit cell. The Fermi surface is fundamentally a circular orbit, but when the orbit intersects the Brillouin zone boundary, the electron is Bragg scattered, opening up a gap of magnitude V_G. As a result of this scattering, the consecutive circular orbits are linked into a pair of open orbits (figure 1(c)). At higher energies, the portion of the circle which has overlapped into the next Brillouin zone emerges as a new, lens-shaped orbital (figure 1(d)). The Fermi surfaces of figure 1(d) are commonly

0953-8984/94/163059+14$19.50

used as an elementary example for studying magnetic breakdown [7–9]. At low transverse magnetic fields, the electrons are confined to cyclotron orbits coinciding with the solid lines of figure 1(d). However, for sufficiently strong fields, the Bragg scattering gap will be a small perturbation, and the electron will follow the free-electron circular orbit (dashed line in figure 1(d)). The crossover between the two orbits is magnetic breakdown. Note that it involves Zener tunnelling between two separate bands, the first-zone open orbit and the second-zone lens orbit [9–11].

On the other hand, orbital switching can be understood with reference to figure 1(a)–(c). Note that an electron that starts at point A with energy E_a (figure 1(a)) will end up at point B with essentially 100% probability, but with energy E_c (figure 1(c)) it will end up at point C with the same probability. Since the bands evolve smoothly in a one-electron picture, there will be an intermediate energy, E_b (figure 1(b)) at which the Fermi surface just touches the Brillouin zone boundary. At this energy, an electron at point A has a finite probability of ending up at either point B or point C. In a semi-classical picture, the probability $P = |p|^2$ of switching from the branch containing point A to branch B would be unity for all $E < E_b$ and zero for all $E > E_b$ (with $Q = |q|^2 = 1 - P$ the probability of switching from A to C). Now the quantum mechanical probability cannot change discontinuously: clearly, when E is less than, but close to E_b, there will be a finite probability of tunnelling through the barrier to branch C. This tunnelling amplitude will be calculated in subsection 2.1. Since P varies smoothly, the switching point E_b can be defined more precisely as that point at which $P = Q = 0.5$.

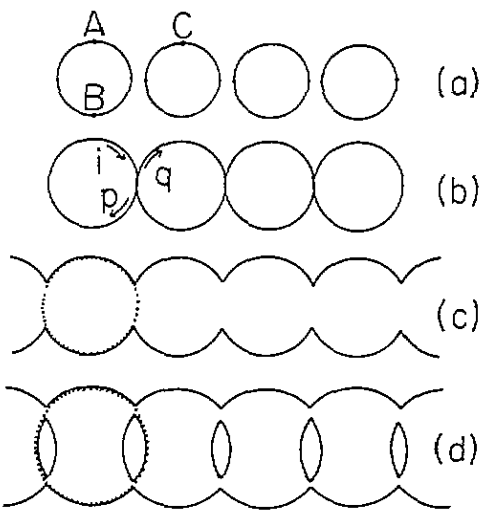

Figure 1. Switching and magnetic breakdown orbits for a linear system (e.g., a material with a rectangular unit cell with one long side). (a)–(d) show the same four cells with successively larger Fermi surfaces (more electrons).

Note the distinctions between orbit switching and magnetic breakdown. First, magnetic breakdown always involves tunnelling through a finite gap, and hence requires a finite magnetic field ($\simeq B_0$, the breakdown field). On the other hand, exactly at the switching point, the tunnelling barrier is zero, so the switching can occur even at zero field. In the calculation of subsection 2.1, the magnetic field will be used to produce electrons with the appropriate velocity to approach the switching point. Any other mechanism of providing

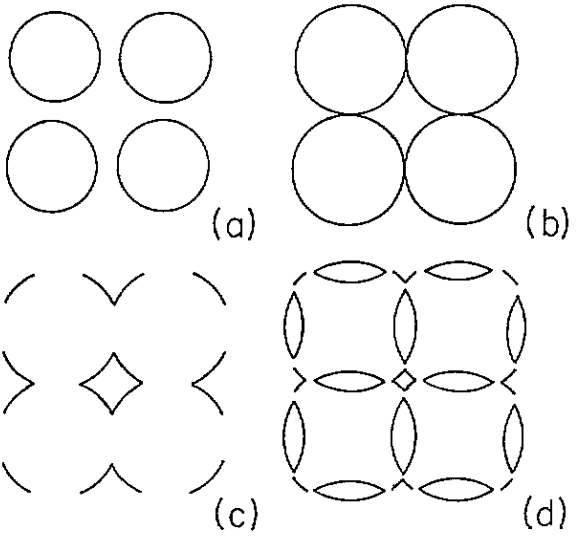

Figure 2. Switching and magnetic breakdown orbits for a two-dimensional system.

the electron with the appropriate velocity (e.g., collision with a thermal phonon or another electron) can initiate the switching event.

Another distinction is that orbit switching involves tunnelling between different parts of a single band, whereas magnetic breakdown couples orbits in two different bands. Because of this, the tunnelling calculation of subsection 2.1 will be distinct from the usual Blount calculation [9] of magnetic breakdown tunnelling. It should be noted that at the switching point, there is also a contribution to the tunnelling due to second-order magnetic breakdown: the electron on branch A can virtually tunnel to the bottom of the lens orbit band, at energy $E_b + V_G$, and then tunnel back down to branch C. The probability for this process will be estimated in subsection 2.2 and appendix B. It will be found that near the switching point, the probability of such conventional magnetic breakdown is actually suppressed below the usual Blount value, and hence can safely be neglected.

Figure 2 shows a two-dimensional version of the same processes. Although this is a nearly free electron model, the Fermi surfaces, particularly in figure 2(a)–(c), bear a close resemblance to the LDA and the tight-binding model approximation to the Fermi surfaces of the high-temperature superconductors, particularly $La_{2-x}Sr_xCuO_4$ (LSCO). While the lens orbits do not arise in the usual three-band model of the CuO_2 planes, the second zone orbital would correspond, in a tight-binding picture, to the Cu $d_{3z^2-r^2}$ orbital. Clearly, the vHs corresponds to the orbital switching point (figure 2(b)).

2. Calculation of the switching amplitude

2.1. Orbit switching

The effect of a saddle point vHs on Landau levels, and the corresponding transmission coefficient (orbital switching probability) have been calculated by several authors [12–14]. Here a simple derivation is presented, leading to a result particularly similar in form to

that of Fertig and Halperin (FH) [14]. Following Onsager's semiclassical approach [15], in the absence of scattering, an electron in a magnetic field travels in a cyclotron orbit in k-space along a section of Fermi surface perpendicular to the magnetic field direction. The real-space orbit is in the same plane and has the same shape, but is rotated by 90° and scaled by a factor $l_B^2 \equiv \hbar c/eB$,

$$r - r_0 = -l_B^2 \hat{z} \times (k - k_0) \tag{1}$$

where r_0 (k_0) is the orbit centre in real (k) space.

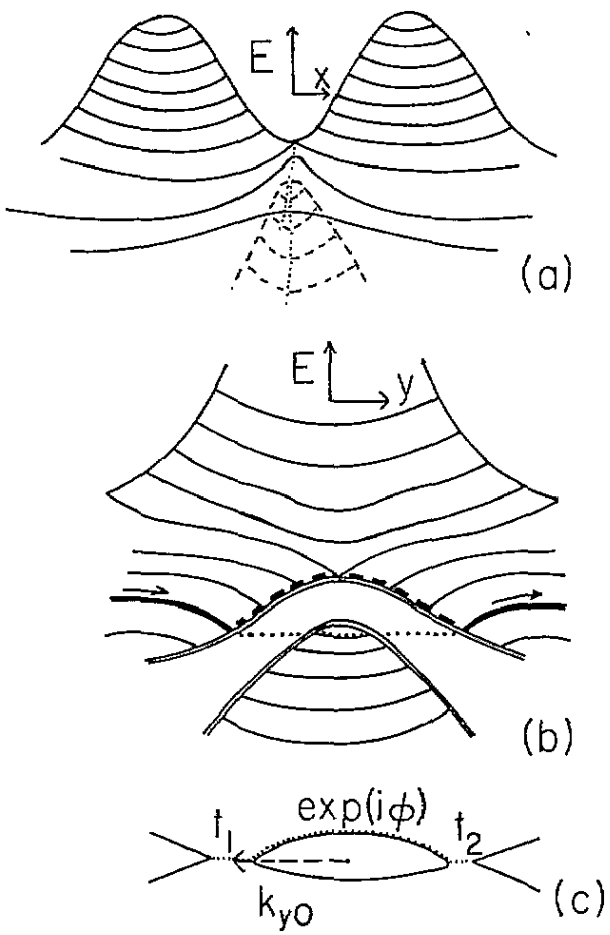

Figure 3. (a) A contour map of real-space magnetic orbitals corresponding to successively larger Fermi surfaces near a switching point. The dashed lines show the second band. (b) A cross-section of the contour map. The double lines are cuts through the surface, corresponding to the dotted lines in (a). The dashed line is tunnelling corresponding to orbit switching; the dotted line is a competing tunnelling path via conventional magnetic breakdown. (c) A single-energy contour corresponding to magnetic breakdown tunnelling (dotted line) in (b).

For studying magnetic breakdown, Pippard [8] has shown that it is convenient to look at the real-space Fourier transform of the full, extended zone scheme—Pippard's O-lattice.

Figure 3(a) shows this real-space transform of two cells from figure 2. This figure shows a series of real-space trajectories of electrons in a fixed magnetic field, for various values of the energy E. Note that two bands are illustrated, the 'lens orbits' (shown as dashed lines) lying below the first band (solid lines). Figure 3(b) is an expanded view of the orbits near one vHs, corresponding to a cut through the energy surface (the double lines in figure 3(b) correspond to the dotted lines in figure 3(a)). Figure 3(b) illustrates two possible tunnelling paths which connect discontinuous orbits of the first band (thick solid lines). The dotted path is the usual, interband (Landau–Zener tunnelling) magnetic breakdown. The dashed curve illustrates the intraband tunnelling associated with a switching orbit. Both tunnelling processes will take place in parallel. For the energy level illustrated in figure 3(b) (lens orbit at the Fermi level, figures 1(d), 2(d)), conventional breakdown will probably predominate, since the double tunnelling into and out of the second band involves a shorter tunnelling path. However, when the energy level approaches closer to the switching point (lens orbit below Fermi level, figures 1(b), (c), 2(b), (c)), the new intraband switching will win out. This latter situation is analysed in the present section, saving conventional magnetic breakdown for subsection 2.2.

The switching involves tunnelling from the initial branch i to the 'transmitted' wave (figure 1(b)), with probability amplitude p, or continuation onto the reflected branch, with amplitude q. The tunnelling problem is thus quasi-1D, and can be solved using a WKB barrier penetration approach. The transmission amplitude can be written

$$p = \mathrm{e}^{-\delta} \tag{2a}$$

$$\delta = \frac{\sqrt{2m}}{\hbar}\int_0^{y_0} \mathrm{d}y\sqrt{E(y) - E_\mathrm{F}} = \frac{l_B^2\sqrt{2m^*}}{\hbar}\int_{-k_{x0}}^{k_{x0}} \mathrm{d}k_x\sqrt{E(k) - E_\mathrm{F}} \tag{2b}$$

with $E(k_x = k_{x0}, k_y = 0) = E_\mathrm{F}$. Near the vHs, the energy can be written

$$E(k) - E_\mathrm{v} = \frac{\hbar^2}{2m^*}(k_x^2 - k_y^2) \tag{3}$$

where E_v is the energy at the vHs (appendix A). Substituting equation (3) (with $k_y = 0$) into equation (2b), the integral can be evaluated, yielding

$$\delta = \frac{\pi E_\mathrm{g}}{\hbar\omega_\mathrm{c}} \tag{4}$$

where $E_\mathrm{g} = E_\mathrm{v} - E_\mathrm{F}$ and $\omega_\mathrm{c} = eB/m^*c$, the cyclotron frequency. Thus, the barrier transmission probability $P = |p|^2$ will become significant when $\hbar\omega_\mathrm{c} > E_\mathrm{g}$. This was the criterion originally introduced for significant magnetic breakdown by Cohen and Falicov [7]. Subsequently, Blount [9] showed that for interband tunnelling the breakdown criterion is actually more favourable,

$$\hbar\omega_\mathrm{c} > V_\mathrm{G}^2/E_\mathrm{F}.$$

In the present circumstance, however, E_g vanishes at the vHs, whereas V_G remains large, so at low fields, the present tunnelling, equation (4), will dominate.

The above WKB approximation implicitly assumed that the tunnelling probability was small. Clearly, this will no longer be the case when E_g is zero or negative. The correct

transmission coefficient can be found by keeping the wave function properly normalized to unity [16]:

$$P = \frac{1}{1 + e^{2\delta}}. \tag{5}$$

Thus, when $E_F = E_v$, $P = \frac{1}{2}$, independent of magnetic field. As the magnetic field increases, there is significant transmission over an ever increasing range of energies away from the vHs. Figure 4 shows plots of P versus E, for several values of magnetic field. Note that P has the form of a Fermi function, with E_v playing the role of chemical potential, and $\hbar\omega_c/2\pi$ the temperature.

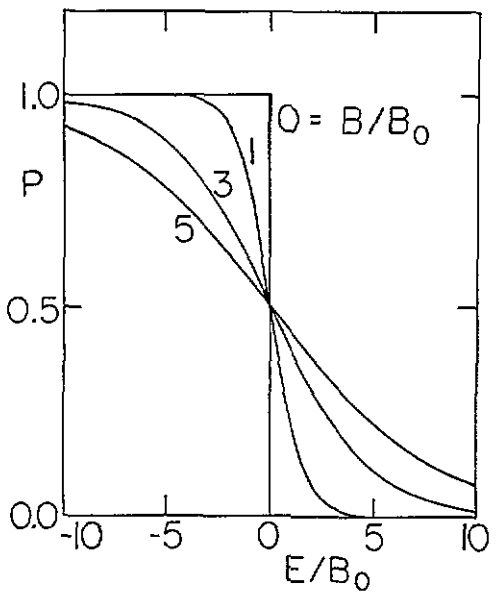

Figure 4. The transmission probability P at a switching orbit, for a variety of magnetic fields. (All fields and energies scaled to a common field, B_0.)

Equation (5) is essentially identical to equation (1.2) of FH. In order to compare the results, the following identifications must be made: for FH's U_x, U_y, $U_x = U_y = \hbar^2/2m^*l_B^4$, so FH's $E_1 \simeq \hbar\omega_c/2$.

2.2. *Conventional magnetic breakdown*

At the same point that the orbital switching mechanism is becoming important, the conventional breakdown mechanism is exponentially suppressed. To see this, it is convenient to follow Dykhne's formalism [17]. The breakdown amplitude is the product of three processes (figure 3(c)): namely breakdown from the left-hand orbit to the lens orbit, t_1; transmission across the lens orbit, represented as $e^{i\phi}$; and a second breakdown from the lens to the right-hand orbit, t_2. The resulting probability amplitude can be written

$$p_{mb} = t_1(e^{i\phi} + r_1r_2r^{3i\phi} + \ldots)t_2$$

where the r_i are the corresponding reflection coefficients, and the terms in the parentheses account for multiple 'internal reflections'. The exponential suppression is contained in both of the breakdown steps; for convenience, only a single breakdown will be considered, $t_{mb} = t_1 = t_2$.

The details of the calculation are given in appendix B. The amplitude for interband tunnelling may be expressed in a form similar to equation (2*a*), $t_{mb} = \exp(-\delta_{mb})$, but with

$$\delta_{mb} = \frac{\beta \pi V_G^2}{\hbar \omega_c E_F} \tag{6}$$

where β is a numerical factor calculated in appendix B. Away from the switching point, $\beta \sim O(1)$, and the tunnelling probability is equivalent to that found by Blount [9]. However, near the switching point β diverges, being ultimately cut off by higher-order terms, and at the switching point $\beta \simeq \sqrt{4E_F/V_G}$, thereby greatly reducing the probability of conventional magnetic breakdown.

2.3. Competition of two tunnelling channels

The distinction between conventional magnetic breakdown and orbital switching can best be understood by comparing (2*b*) and (B1). These may be written schematically as

$$\hbar \delta_{os} \sim \int \Delta p \, dx \tag{7a}$$

$$\hbar \delta_{mb} \sim \int \Delta E \, dt. \tag{7b}$$

That is, orbital switching (os) corresponds to tunnelling in space, and magnetic breakdown (mb) to tunnelling in energy. The two modes are associated with the two forms of the uncertainty principle,

$$\Delta x \, \Delta p \geqslant \hbar/2 \qquad \Delta E \, \Delta t \geqslant \hbar/2.$$

An analogous situation arises in variable-range hopping [18]. There, a competition arises between direct space tunnelling (long-range hopping) and energy activation to the mobility edge. The anomalous temperature dependence of the hopping conductivity arises from optimization of the hopping range between these two competing tunnelling paths. The magnetic breakdown problem differs in that the range is essentially fixed by the interorbital separation, and the energy activation is not to a mobility edge, but to another orbital.

3. Consequences of the switching orbit

3.1. Switching lattice

It might be thought that orbit switching or magnetic breakdown would lead to strong electronic disorder. For instance, for the orbits of figure 2(b), it appears that $\omega_c \tau \leqslant \pi/4$ (with τ a scattering time), since an electron is scattered each time it reaches a switching point. In fact, Pippard [8] has shown that this is not the case. When $\omega_c \tau' \gg 1$ (with τ' the scattering time exclusive of switching point scattering), the tunnelling produces a

quantum coherent structure: there is a well defined magnetic band structure, associated with a magnetic superlattice. (Pippard analysed in detail only the case in which the magnetic field was 'commensurate' with the real-space lattice.) For ordinary magnetic breakdown, the transmission probability is strongly field dependent, $T \sim \exp(-B_0/B)$, so this lattice only exists in a limited range of magnetic fields. Moreover, magnetic breakdown is usually observed in three-dimensional metals, where it involves only a small fraction of the Fermi surface, leaving a large background of carriers not involved in the breakdown orbits. Hence, coherent magnetic breakdown has only occasionally been observed experimentally [19].

In contrast, T at the switching point is $\frac{1}{2}$, independent of field (until true magnetic breakdown across V_G becomes significant), so the 'switching lattice' will persist out to quite high fields, $\omega_c\tau \gg 1$. Moreover, in a quasi-two-dimensional lattice, the switching will involve nearly all the conduction electrons, leading to inherently larger effects with weaker backgrounds [20]. The disadvantage is that, since the vHs occurs near a half filled band, the effective masses will be close to a free electron mass, or even somewhat larger, necessitating the use of very high magnetic fields. Nevertheless, these fields do not seem out of the range of current capabilities [21]. For the model of figure 2, the energy dispersion in the switching lattice is calculated in appendix C.

3.2. Excitonic effects and anomalous Hall effect

The presence of switching orbits at the vHs was pointed out earlier [22], and some of the consequences noted: there is a simultaneous presence of electron-like and hole-like orbits at the Fermi level, leading to unusual excitonic effects [23]; and the switching leads to anomalous values for the Hall coefficient [20]. The Hall effect is known to be anomalous in the cuprate superconductors: whereas photoemission finds evidence for large ('Luttinger') Fermi surfaces, the measured Hall density only corresponds to the excess holes beyond half filling of the band. A low-field Hall effect calculation [20] suggests that the switching orbit, coupled with strong correlation effects, may be able to account for this anomaly.

4. Discussion

4.1. Weakly coupled chains

Away from a switching point, all of the orbits are closed in k-space, and hence the real-space orbitals (1) are all localized in a strong field. In contrast, at a switching orbit, the electron can follow an open orbit path which percolates throughout momentum space and, hence, throughout real space. In particular, figure 5, an expanded view of figure 2(b), illustrates the existence of quasi-1D orbitals.

This suggests a novel interpretation for orbital switching. At a point at which orbital switching occurs, the two-dimensional band can be thought of as composed of *two interpenetrating, weakly coupled chains*. Thus, the dotted and dashed orbitals in figure 5 represent two essentially 1D chains, at right angles to each other. Clearly, the whole lattice can be represented as a superposition of such chains. A similar association of the vHs with one dimensionality was made earlier [24].

Anderson [25] has suggested that such a state could have important consequences for high-T_c superconductivity. He has pointed out that, due to correlation effects, 1D metals have a number of highly anomalous properties, including separation of spin and charge degrees of freedom, which could lead to a novel form of superconductivity. In trying to extend models of these 'Luttinger liquids' to two dimensions, he has suggested that correlation

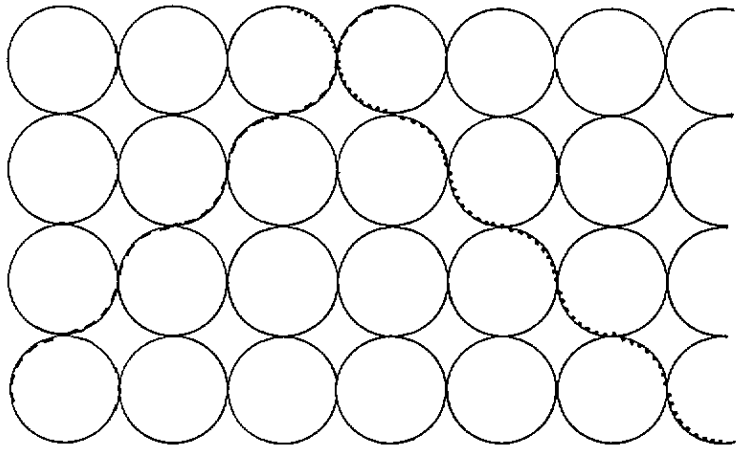

Figure 5. An interpretation of switching orbit in terms of weakly coupled chains. The dashed and dotted lines show two interpenetrating, essentially 1D orbits, at right angles to each other.

effects can make interchain hopping irrelevant [25], so the resulting weakly coupled chains will retain the characteristic features of a Luttinger liquid.

The present result suggests that such weakly coupled chains arise naturally, but only in the *middle* of a 2D band, due to the presence of vHs switching orbits. It may be that near the extrema of the band, interchain hopping remains relevant, its importance enhanced because the DOS of a 1D band diverges at the top and bottom of the band (due to 1D vHs).

4.2. vHs scattering in zero field

Orbital switching is inherently easier to analyse in a magnetic field, because the field forces the carriers to travel along well defined orbits, with the tunnelling occuring at precise turning points of the orbits. However, since orbital switching persists to zero field, it can also be thermally activated. That is, there will be an additional scattering mechanism present for carriers near the vHs of the Fermi surface. Moreover, phonons can cause inter-vHs switching in addition to the single-vHs switching discussed above. For these reasons, the present discussion is limited to magnetic field dependence, both to introduce the phenomenon of orbital switching and to clarify the distinction between switching and magnetic breakdown. Nevertheless, there is evidence in the high-T_c cuprates for coherent electron–phonon coupling, in the form of dynamic Jahn–Teller effects [24]. A description of these effects in terms of phonon-assisted orbital switching is currently being prepared.

Acknowledgments

I thank P Argyres and J Jose for stimulating discussions, and J Jose for suggesting the analogy with variable-range hopping. This paper is publication 575 of the Barnett Institute.

Appendix A. Band dispersion near the vHs

In the high-temperature superconducting cuprates, the CuO_2 antibonding band is often represented in a tight-binding model, with dispersion

$$E = \frac{\Delta}{2} + \sqrt{\left(\frac{\Delta}{2}\right)^2 + 4t_{\mathrm{CuO}}^2\left(\sin^2\left(\frac{k_x a}{2}\right) + \sin^2\left(\frac{k_y a}{2}\right)\right)}. \tag{A1}$$

Here, Δ is the Cu–O bare energy separation, t_{CuO} is the Cu–O hopping energy, and a is the in-plane lattice constant. The vHs corresponds to $(k_x, k_y) = (0, \pi)$, or

$$E_{\mathrm{v}} = \frac{\Delta}{2} + \sqrt{\left(\frac{\Delta}{2}\right)^2 + 4t_{\mathrm{CuO}}^2}. \tag{A2}$$

Near the vHs ($k_x \sim 0$, $k_y = \pi - k_y'$), the energy may be expanded as

$$E = E_{\mathrm{v}} + \frac{\hbar^2}{2m^*}(k_x^2 - k_y'^2) \tag{A3a}$$

$$\frac{\hbar^2}{m^*} = \frac{t_{\mathrm{CuO}}^2 a^2}{\sqrt{(\Delta/2)^2 + 4t_{\mathrm{CuO}}^2}}. \tag{A3b}$$

Using the values $\Delta \sim 4$ eV, $t_{\mathrm{CuO}} \sim 1.3$ eV, $a = 3.8$ Å, m^* is close to the free electron value. Correlation effects tend to reduce the Cu–O hopping, t_{CuO}, and hence to enhance m^*.

Appendix B. Conventional magnetic breakdown near a vHs

In this appendix, the calculation of the tunnelling matrix element t_{mb} of figure 3(c) is presented. Following Dykhne [17], t_{mb} can be written as earlier, but with

$$\delta = \mathrm{Im}\int_0^{t_{\mathrm{c}}} \frac{(E_+ - E_-)}{\hbar}\mathrm{d}t \tag{B1}$$

where $E_\pm$ are the energies of the two bands, and t_{c} is the (imaginary) time it takes to go from one to the other.

To calculate δ, it is necessary to know the extrapolation of E to complex values. In general, the degeneracy point will usually be associated with a point of conical intersection. In the present spirit of nearly free electron bands, the following model suggests itself (however, the final result is not sensitive to the details of the model). Where two Fermi surface sections of figure 1 or 2 overlap, umklapp scattering will introduce a gap. The resulting wave function will be a combination of

$$\Phi = c_k \mathrm{e}^{\mathrm{i}k\cdot r} + c_{k+G_1}\mathrm{e}^{\mathrm{i}(k+G_1)\cdot r} \tag{B2}$$

with $G_1 = (G_1, 0)$, and all vectors are two dimensional. The eigenenergies are given by the roots of

$$\det\begin{pmatrix} \lambda_k - E & U_{\mathrm{G}} \\ U_{\mathrm{G}} & \lambda_{k-G_1} - E \end{pmatrix} = 0 \tag{B3}$$

with $\lambda_k = \hbar^2 k^2/2m$, and U_{G} the interband coupling energy. Letting $k_x = G_1/2 - \kappa_x$, the energies are

$$E_\pm = E_0 \pm E_1 \tag{B4a}$$

$$E_1 = \sqrt{4\lambda_G \frac{\hbar^2 \kappa_x^2}{2m} + U_G^2} \tag{B4b}$$

with

$$E_0 = \hbar^2[(G_1/2)^2 + \kappa_x^2 + k_y^2]/2m$$

and

$$\lambda_G = \hbar^2 G_1^2/2m.$$

To transform from time to wave number, use the equation of motion

$$\frac{\partial \kappa_x}{\partial t} = \omega_c k_y \tag{B5}$$

with $\omega_c = eB/mc$. Thus,

$$dt = \frac{d\kappa_x}{\omega_c k_{y0}} \tag{B6}$$

where k_{y0} is the value of k_y at the gap (figure 3(c)). The interband tunnelling is accomplished by letting κ_x (or t) take on imaginary values ranging from 0 to $i\kappa^*$, with

$$\hbar\kappa^* = U_1\sqrt{\frac{m}{2\lambda_G}} \tag{B7}$$

(i.e., with $E_1 = 0$). Carrying out the integral, equation (B1) now yields

$$\delta = \frac{\pi U_1^2 G_1}{\hbar\omega_c \lambda_G k_{y0}}. \tag{B8}$$

Equation (B8) is essentially equivalent to the Blount result. Thus, the energy gap is $V_G = 2U_1$, so by identifying the Fermi energy as $E_F \simeq \lambda_G$, equation (B8) becomes

$$\delta = \frac{\beta\pi V_G^2}{\hbar\omega_c E_F}$$

with $\beta = G_1/4k_{y0}$. For $\beta = 1$, this expression exactly agrees with Blount's version. However, as the orbital switch is approached, $k_{y0} \to 0$, $\beta \to \infty$, and the ordinary breakdown mechanism is strongly suppressed. In this limit, a finite tunnelling probability can be restored by a higher-order approximation for equation (B5). For a circular nearly free electron orbit, $k_x = (G_1/2)\cos(\omega_c t)$, so

$$\kappa_x = (G_1/2)(1 - \cos(\omega_c t)) \simeq (G_1/4)(\omega_c t)^2$$

near the switching orbit. Substituting this in (B1), (B4) yields

$$\delta = \frac{\pi\eta U_1^2}{\hbar\omega_c\lambda_G} \tag{B9a}$$

$$\eta = \frac{2\eta_0}{\pi}\sqrt{\frac{2\lambda_G}{U_1}} \tag{B9b}$$

with

$$\eta_0 = \int_0^1 (1 - x^4)\, dx = (\sqrt{2}/3)K(1/\sqrt{2}) \simeq 1.180$$

with K the complete elliptic integral of the first kind. Thus, up to a small numerical factor, the divergent quantity G_1/k_{y0} is replaced by the large but finite $\sqrt{4E_F/V_G}$. Therefore, near the orbital switch, the space-like tunnelling, equation (4), is expected to dominate over the energy-space tunnelling, equation (B9).

Appendix C. Magnetic band structure at the vHs

The 'switching lattice' energy dispersion may be calculated, following the calculations of Pippard [8] for magnetic breakdown. It is assumed that scattering by impurities, phonons, etc (i.e., all scattering except that associated with the switching points) is negligible, $\omega_c\tau' \gg 1$. In this limit, an electron in a strong magnetic field follows a well defined semiclassical orbit, with the phase of the wave function increasing in proportion to the area swept out divided by the magnetic area, $l_B^2 = \hbar c/eB$. At a switching point, this unique characterization breaks down, and the electron entering a switching point has two possible paths: it can either emerge on the 'same' orbit, with probability amplitude q, or switch to an alternative orbit, with probability amplitude p. Pippard [8] makes the conventional choice of taking q as a real number, and

$$p = ip_0 = i\sqrt{1-q^2}.$$

Thus, in figure 6, the wavefunctions on any branch of the orbit can be uniquely specified with respect to the wavefunctions at the centre points of the branches, A, B, C, and D.

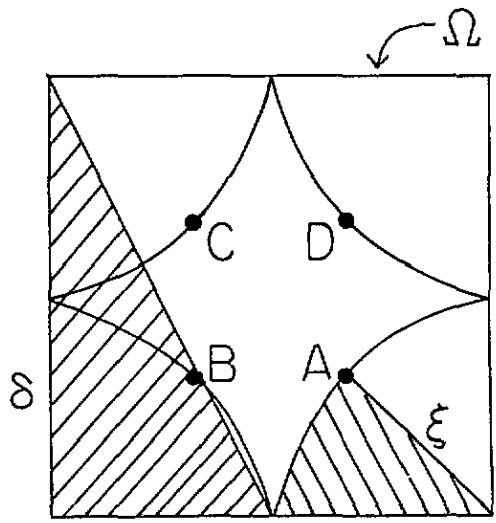

Figure C1. Definition of arc centres (A–D) and orbit areas (ξ, δ, and Ω, the entire cell) for use in calculation of the 'switching lattice' energy dispersion.

An equation relating the wavefunction at B to those at A and C can be found by following the time evolution of the wavefunction backwards from point B:

$$Be^{-i\xi} = qAe^{i\xi} + pCe^{i(\xi+\delta-\omega_x)}. \tag{C1a}$$

The phase factors in this equation have the following origins. The term $\xi = A_\xi/l_B^2$ is the phase picked up by moving from A to the switching point, corresponding to the area labelled ξ in figure 6 (with analogous areas for branches B, C). Here A_ξ is the real-space area of the orbit section. The term $\omega_x = k_x a_s$ is an extra phase picked up by shifting from point C to the equivalent point in the next cell, with $a_s = 2ma$ the length of the magnetic supercell (a is the cell parameter of the atomic lattice, and m is an integer specifying the size of

the magnetic supercell, discussed further below). The factor δ must be introduced due to a gauge transformation associated with switching the orbit centre [8], and corresponds to the area δ in figure 6. (The vector potential can be written $\boldsymbol{A} = (\boldsymbol{B} \times \boldsymbol{r})/2$. When $\boldsymbol{r}$ is identified as the centre of a given orbit, the electronic phase is given by the area swept out, as described above. However, any change in the orbit centre is equivalent to redefining $\boldsymbol{A}$—i.e., is a gauge transformation.)

Equivalent equations can be written for the other wavefunctions:

$$Ce^{-i\xi} = qBe^{i\xi} + pDe^{i(\xi+\delta+\omega_y)} \tag{C1b}$$

$$De^{-i\xi} = qCe^{i\xi} + pAe^{i(\xi+\delta+\omega_x)} \tag{C1c}$$

$$Ae^{-i\xi} = qDe^{i\xi} + pBe^{i(\xi+\delta-\omega_y)}. \tag{C1d}$$

This system of equations can be solved when the magnetic field is commensurate—that is, when the crystallographic unit cell contains a magnetic flux equal to $1/2m$ of a flux quantum hc/e, where m is an integer. Equivalently, the magnetic unit cell has an area equal to $2m$ times that of the crystallographic cell. For a commensurate field, the phase corresponding to a circuit of the entire Brillouin zone is $\Omega = 4\pi m$, so $\delta = \Omega/4 = \pi m$ and $8\xi = (1+x)\Omega/2$, where x is the equivalent hole doping (i.e., $x = 0$ corresponds to a half-filled band, $x = 1$ to the whole band filled with holes).

In this commensurate case, equation (C1) is a 4×4 matrix equation, and the dispersion of the magnetic bands is found by equating the determinant of this matrix to zero. This yields

$$\cos(k_x a_s) + \cos(k_y a_s) = -\frac{\sin(\pi m x)}{q p_0} \tag{C2}$$

where $p_0 = \sqrt{1-q^2}$. Note that for $x = 0$, this is very similar to the usual equation for the Fermi surface associated with the vHs in zero field,

$$\cos(k_x a) + \cos(k_y a) = 0.$$

References

[1] Hirsch J E and Scalapino D J 1986 *Phys. Rev. Lett.* **56** 2732
[2] Labbe J and Bok J 1987 *Europhys. Lett.* **3** 1225
[3] Dzyaloshinskii I E 1987 *Zh. Eksp. Teor. Fiz.* **93** 1487 (Engl. Transl. 1987 *Sov. Phys.–JETP* **66** 848)
[4] Friedel J 1989 *J. Phys.: Condens. Matter* **1** 7757
[5] Markiewicz R S 1991 *Int. J. Mod. Phys.* B **5** 2037
[6] Newns D M, Tsuei C C, Pattnaik P C and Kane C L 1992 *Comment. Condens. Matter Phys.* **15** 273
[7] Cohen M H and Falicov L M 1961 *Phys. Rev. Lett.* **7** 231
Falicov L M and Sievert P M 1965 *Phys. Rev.* **138** A88
[8] Pippard A B 1965 *Proc. R. Soc.* A **287** 165
[9] Blount E I 1962 *Phys. Rev.* **126** 1636
[10] Zener C 1934 *Proc. R. Soc.* A **145** 523
[11] Kane E O 1959 *J. Phys. Chem. Solids* **12** 181
[12] Azbel M Ya 1960 *Zh. Eksp. Teor. Fiz.* **39** 1276 (Engl. Transl. 1961 *Sov. Phys.–JETP* **12** 891)

[13] Giura M and Wanderlingh F 1968 *Phys. Rev. Lett.* **20** 445
[14] Fertig H A and Halperin B I 1987 *Phys. Rev.* B **36** 7969
[15] Onsager L 1952 *Phil. Mag.* **43** 1006
[16] Landau L D and Lifshitz E M 1958 *Quantum Mechanics* (London: Pergamon) p 177
[17] Dykhne A M 1961 *Zh. Eksp. Teor. Fiz.* **41** 1324 (Engl. Transl. 1962 *Sov. Phys.–JETP* **14** 941)
Moody J, Shapere A and Wilczek F 1989 *Geometric Phases in Physics* ed A Shapere and F Wilczek (Singapore: World Scientific) p 160
[18] Mott N 1974 *Metal–Insulator Transitions* (London: Taylor & Francis)
[19] Stark R W and Reifenberger R 1977 *J. Low Temp. Phys.* **26** 753
Sandesara N B and Stark R W 1985 *Phys. Rev. Lett.* **53** 1681
[20] Markiewicz R S 1991 *Physica* C **177** 445; 1993 *Physica* C **207** 281
[21] Mueller F M, Fowler C M, Freeman B L, Hults W L, King J C and Smith J L 1991 *Physica* B **172** 253
[22] Markiewicz R S 1989 *J. Phys.: Condens. Matter* **1** 8911
[23] Markiewicz R S 1991 *J. Phys.: Condens. Matter* **3** 3859
[24] Markiewicz R S 1992 *Physica* C **193** 323, **200** 65; 1993 *Physica* C **210** 235, 264
[25] Anderson P W 1991 *Phys. Rev. Lett.* **67** 3844
See also
Guinea F and Zimanyi G 1993 *Phys. Rev.* B **47** 501